Short Communication

Gas Sensing and Electrochemical Behaviors of Ag-doped 3D Spherical WO₃ Assembled by Nanostrips to Formaldehyde

Huimin Yu, Jianzhong Li[*], Yanwen Tian, Zaiyuan Li

School of Metallurgy, Northeastern University, Shenyang 110819, China
[*]E-mail: lijz@smm.neu.edu.cn, yuhuimin-neu@outlook.com

A novel Ag-doped WO₃ sensing material was successfully prepared via a facile hydrothermal method combining with a wet dipping process. The phase composition and micromorphology of the as-obtained samples were characterized by X-ray diffraction (XRD) and field emission scanning electron microscope (SEM) technology. The electrochemical behavior and sensing were investigated, the results demonstrated that the vibration in resistance of Ag-doped WO₃ was approximately 3.5 times higher than the pure one after contacting formalin, and a higher response of 10.3 to 100 ppm HCHO was exhibited at working temperature of 250 °C, which was better than the pure WO₃ of 6.5 at 350 °C, the response/recovery time was shorted to 3 s/3 s. The enhanced of gas sensing behavior of WO₃ after introducing Ag could be attributed to the hetero-structure and the catalysis role of silver. The Ag-doped WO₃ is expected to be a promising in HCHO gas-sensing practical applications.

1. INTRODUCTION

For the past years, with the sustained and rapid social economic development, environmental pollution and other issues that accompany it were also worthy of attention. Especially the series of problems such as the human health, the formation of acid rain, the destruction of the ozone layer, and the warming of the climate caused by poisonous and pernicious gases released by coal, factories, and more motor vehicles. Therefore, it's extremely necessary to monitor these toxic and harmful gases effectively in real time. Formaldehyde, as a major indoor pollution gas, is mainly released from wooden furniture, textiles, paints, coatings and even food preservatives. It has caused great threat to the human respiratory system and immune system, and was identified as the No.1 types of carcinogen by International Agency for Research on Cancer (IARC) in 2006, therefore, more attention should be paid to the detection of formaldehyde.

Up to now, metal oxide semiconductor (MOS) -based solid-state gas sensors have attracted many more attentions to detect toxic gases because of their convenient carrying, simple production process, low production cost, and excellent gas-sensing performances, and it has great development prospects for practical application and industrial production. MOS materials such as SnO_2 [1-4], ZnO [5-7], WO_3 [8-10] have all been reported for monitoring poisonous/inflammable or explosive gas including ethanol, H_2S, or volatile organic compounds (VOCs). It has been proved that pure MOS material may have the disadvantages of high working temperature, slow response/recovery speed or poor sensitivity, so doping noble metal nanoparticles can be used to achieve the enhancement on gas sensing performances [1-2,7]. As we all know that the gas sensing properties of MOS-based gas sensors are strongly related to the size and morphology of the material. In recent years, one-dimensional (1D) nanostructure such as nanorods, nanowires, nanofibers [8,10,11], two-dimensional (2D) such as nanosheets [12], and three-dimensional (3D) nanostructure such as nanoflowers [2,13] were all investigated to for application in gas sensitive materials. Compared with the other two kinds of nanostructures, 3D nanomaterials have a large specific surface area and rich channels, which are beneficial to the adsorption and transport processes of gas molecules, thus attracting more extensive attention and research.

As a typical n-type semiconductor, WO_3 has been widely used in gas-sensitive materials, photocatalysts, electrochromic materials and supercapacitors [12,14] due to its excellent chemical and physical properties. Supported noble metal catalysts such as Pd, Pt, Au are regarded to be suitable to detect reducing gas. However, the high costs limit their practical application. By comparison, the much cheaper noble metal Ag are more compatible for actual application.

Herein, in our present work, we reported a facile hydrothermal method without any toxic regents to synthesis hollow spherical WO_3 assembled by nanostrips, and Ag was selected as a reasonable precious metal dopant to 3D spherical WO_3. Sensing performances of the novel gas sensor based on the as-obtained materials were tested and compared on exposure to target formaldehyde gas. The effect of Ag-doping was analyzed and the possible sensing mechanism was also discussed.

2. EXPERIMENTAL

2.1 Chemical and regents

In this experiment, Sodium tungstate ($Na_2WO_4 \cdot 2H_2O$, Mw = 329.86), oxalic acid ($H_2C_2O_4 \cdot 2H_2O$, Mw = 126.04), hydrochloric acid (HCl, 36% - 38%), polyvinylpyrrolidone (PVP K-30, Mw = 40,000), silver nitrate ($AgNO_3$, Mw = 169.87), L-ascorbic acid ($C_6H_{14}N_2O_2$, Mw = 146.19) and formalin solution (HCHO, 37%) purchased from Sinopharm Chemical Regent Co. Ltd. were all of analytical grade and used without any further purification. Deionized water was used throughout all the experiments.

2.2 Preparation of WO₃ spherical

3D WO_3 spherical assembled by nanostrips was prepared by a hydrothermal menthod as below: 0.02 mmol of $Na_2WO_4 \cdot 6H_2O$ was dissolved in 100 mL deionized water firstly, and under vigorous stirring for 30 min at room temperature to form a homogenous solution A. Meanwhile, 0.02 mmol of $H_2C_2O_4 \cdot 2H_2O$ was dissolved in 30 mL deionized water under magnetic stirring to obtain solution B. Then, solution B was slowly added to solution A to get solution C, 3 M HCl aqueous solution was gradually added to adjust the pH value of solution C to 1 ~ 1.5 at ambient temperature. After making a homogenous solution, the mixture was transformed into a 200 mL Teflon-lined stainless steel autoclave and maintained at 150 °C for 12 h. After cooling to room temperature, the resulting precipitate was centrifuged and alternately washed with water and ethanol for several times, and then dried at 60 °C for 12 h in an oven to obtain the precursor. Finally, the dried precursor was calcined in the muffle furnace at 400 °C for 2 h to obtain the yellow solid products WO_3 nanomaterials.

2.3 Synthesis of Ag-doped WO_3 spherical

To decorate Ag nanoparticles on WO_3 spherical surfaces, typically, 2 g of the as-obtained WO_3 spherical were first ultrasonically dispersed in a 50 ml mixture solution containing deionized water (H_2O) and absolute ethanol with a volume ratio of 1:1 for 15 min, and then, 0.6 g PVP K-30 and a certain quality of 0.01 M $AgNO_3$ were added into the above solution. After that, 10 ml L-ascorbic acid (0.05 M) was added into the above solution at 40 °C for 3 h, resulting in the deposition of Ag nanoparticles on WO_3 spherical' surface. The products were collected by centrifugation and then dried in an oven for 24 h after washing several times with deionized water and absolute ethanol. Ag@WO_3 spherical were obtained by calcining the drying production at 400 °C in air for 1 h for further removal of undesirable substances.

2.4 Characterization of materials

The phase and crystallinity of the products were analyzed by powder X-ray diffraction (XRD) on a Rigaku UItima IV diffractometer using Cu-Kα radiation (λ=1.5406 Å) operated at a voltage of 40 kV and a current of 40 mA over the 2θ range of 10~90° with a scanning speed of 5°/min. Morphologies of the products were characterized by field emission scanning electron microscope (FESEM, ZEISS ULTRA PLUS, Germany). Energy dispersive X-ray spectrogram (EDX) measurement were performed on an Oxford X-Max 50 to analyze the elemental composition of the samples. CHI 660B electrochemical workstation (CH Instrument Co. China) was used to measure electrochemical impedance spectroscopy (EIS) analysis.

2.5 Fabrication and testing of sensor

The step of fabricating gas sensor devices can be described as follows: the obtained samples were uniformly dispersed into a moderate amount of deionized water under grinding processing to get a well-dispersed slurry, which was then painted onto an Al_2O_3 ceramic tube (4 mm in length, 2 mm in

diameter) with a pair of Au electron contacted with four Pt lead wires to obtain a sensing films. After being annealed in muffle furnace at 400 °C for 1 h, a Ni-Cr alloy wire was inserted through the ceramic tube to act as a heater to control the working temperature of sensing films, and then the ceramic tube was welded onto a six-probe pedestal to complete the preparation process. The as-fabricated gas sensors were aged at 340 °C for 5 days in aging equipment to enhance stability and repeatability before testing the gas sensing performances

The sensor signal voltage (V_{out}) was monitored by a computer at a text circuit voltage of 5 V. For a typical n-type semiconductor, the sensing response of gas sensors toward reducing gas was defined as $S = R_a/R_g$, where R_a and R_g stand for the electrical resistance in air and in target gas, respectively. The response and recovery time were defined as the time consumed by the sensor to reach 90% of the change in total resistance in case of detected gas adsorption and desorption, separately. All the experiments were conducted at an ambient temperature of 25 °C and the relativity humidity of the test environment was 25% ~ 40% RH.

2.6 Electrochemical tests

The electrochemical sensing behaviors of the as-obtained WO_3 and Ag-doped WO_3 were evaluated by a three-electrode system. The samples coated on a copper sheet were used as working electrode (WE), platinum sheet and mercurous chloride electrode (KCl, saturate) acted as the counter electrode (CE) and reference electrode (RE), separately. All the tests were performed in 0.5 M H_2SO_4 solution.

3. RESULTS AND DISCUSSION

3.1 Characterization of the samples

The phase and crystallinity of the as-prepared samples were confirmed by X-ray diffraction (XRD) pattern, and the diffraction pattern of the precursor product obtained by hydrothermal was shown in Fig. 1. The sharp diffraction peaks and high intensity suggested the high crystallinity of the precursor products, and all of the diffraction peaks in XRD pattern could be indexed to orthorhombic phase of $WO_3 \cdot H_2O$ and $WO_3 \cdot 0.33H_2O$, demonstrating the precursor were the mixture of two phases structure. Fig. 2 successively exhibits the XRD pattern of the calcined products and the as-obtained Ag-doped samples. It's obviously to see that the samples were well crystalline and the deflection peaks of calcined precursor can be readily indexed to the orthorhombic and hexagonal WO_3, indicating the precursor was fully dehydrated under calcining process and the obtained WO_3 was a combination of two phases structure. In the case of the pattern of Ag-doped WO_3, the product was still a mixed crystal of orthorhombic and hexagonal structure WO_3. The addition of silver does not obviously change the crystalline structure of the material, only the intensity of the (002) crystal surface was obviously enhanced, which may be due to the continued selective growth of the (002) crystal surface during the

process of silver loading. The characteristic peak positioned at 38.1° was indicative of (111) facets of cubic Ag, which was marked with a blue pentagram.

The morphologies of the obtained samples were further characterized by scanning electron microscopy, the SEM images are shown in Fig. 3. The images in Fig. 3(a-b) clearly confirmed the WO_3 precursor product obtained by hydrothermal reaction is a 3D spherical structure self-assembled of regular nanostrips with a thickness of 90 ~200 nm. As observed in Fig. 3(c-d), the dehydrated precursor product still shows a spherical morphology assembled by nanostrips.
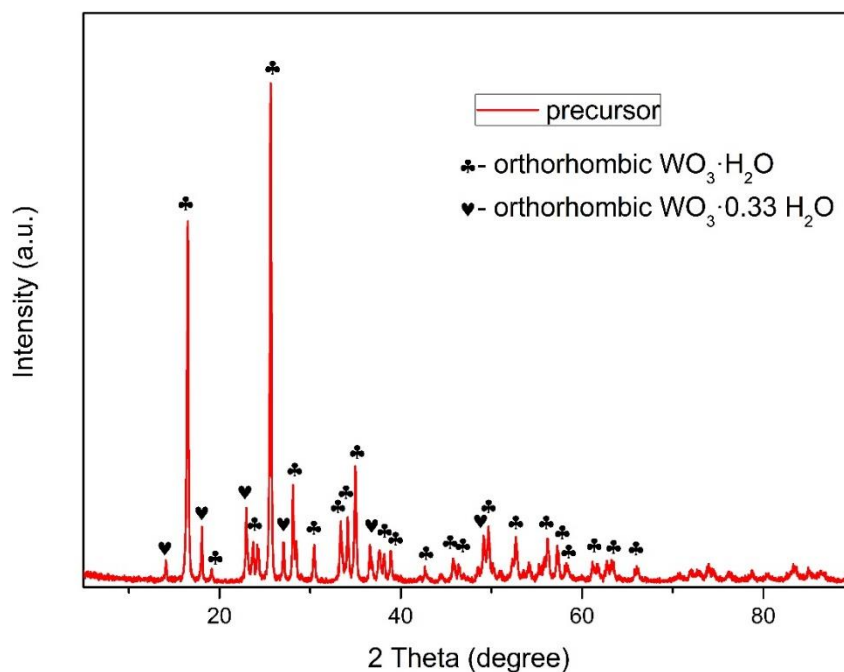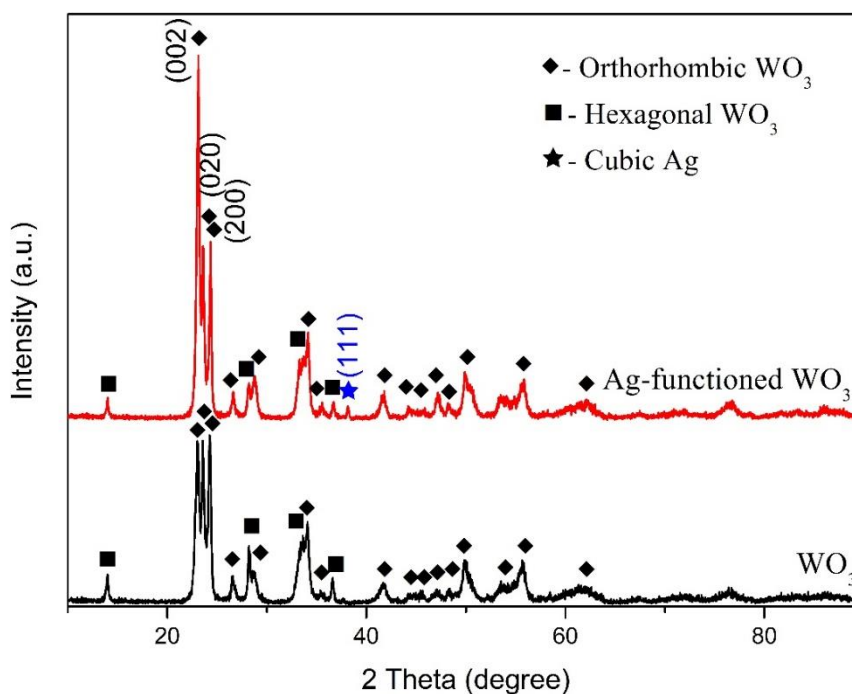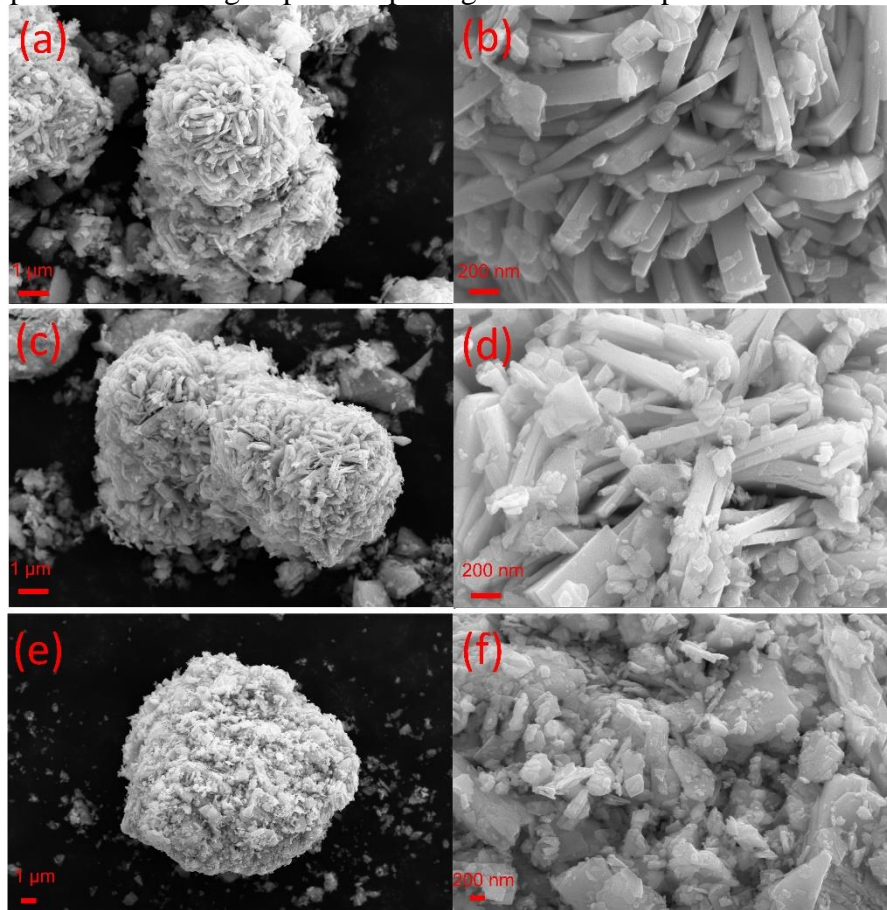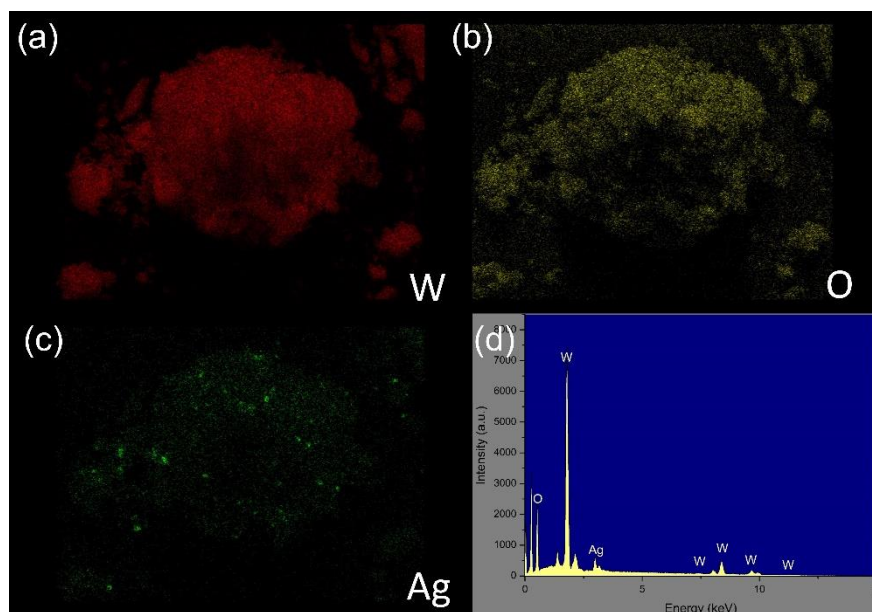
Figure 1. XRD pattern of hydrothermal precursor product

Figure 2. XRD patterns of the Ag-doped sample together with the precursor after calcining at 400 °C

Figure 3. SEM images (a-b) WO$_3$ precursor (c-d) WO$_3$ precursor after calcining at 400 °C (e-f) Ag-doped WO$_3$


Figure 4. Elemental mapping of Ag-doped WO$_3$ sphere (a) W map (b) O map (c) Ag map and (d) EDS spectrum of Ag-doped WO$_3$ sphere

Although the nanostrips are slightly broken after sintering, the clear interlaced strips can still be seen distinctly. Ag-doped WO_3 also exhibits 3D spherical morphology as shown in Fig. 3(e-f), and it is believed that the addition of silver causes the surface of the nanostrips to be covered by small particles, the loose structure and the catalysis of silver are conducive to the transmission of gas. The EDS elemental mapping of Ag-doped WO_3 hierarchical microsphere shown in Fig. 4, confirming that only W, O and Ag elements were contained in the sample and Ag was distributed throughout the WO_3 framework uniformly.

3.2 Electrochemical analysis

Electrochemical behaviors of WO_3 and Ag-doped WO_3 have been investigated. In this report, we have used a three-electrode system for electrochemical testing, all the electrochemical tests were conducted at room temperature. Different electrochemical properties are expected to exhibit before and after exposure to a reducing formalin liquid due to the changes in the structure of the material after doping Ag. The EIS results of the as-prepared samples were performed in solution with containing or without formalin solution to study the sensing mechanism, and the comparison of variation in capacitance as Nyquist plotted in Fig. 5. We can clearly observe that the capacitance of WO_3 and Ag-doped WO_3 have all decreased after contacting formaldehyde, confirming the materials were typical N-type semiconductor.
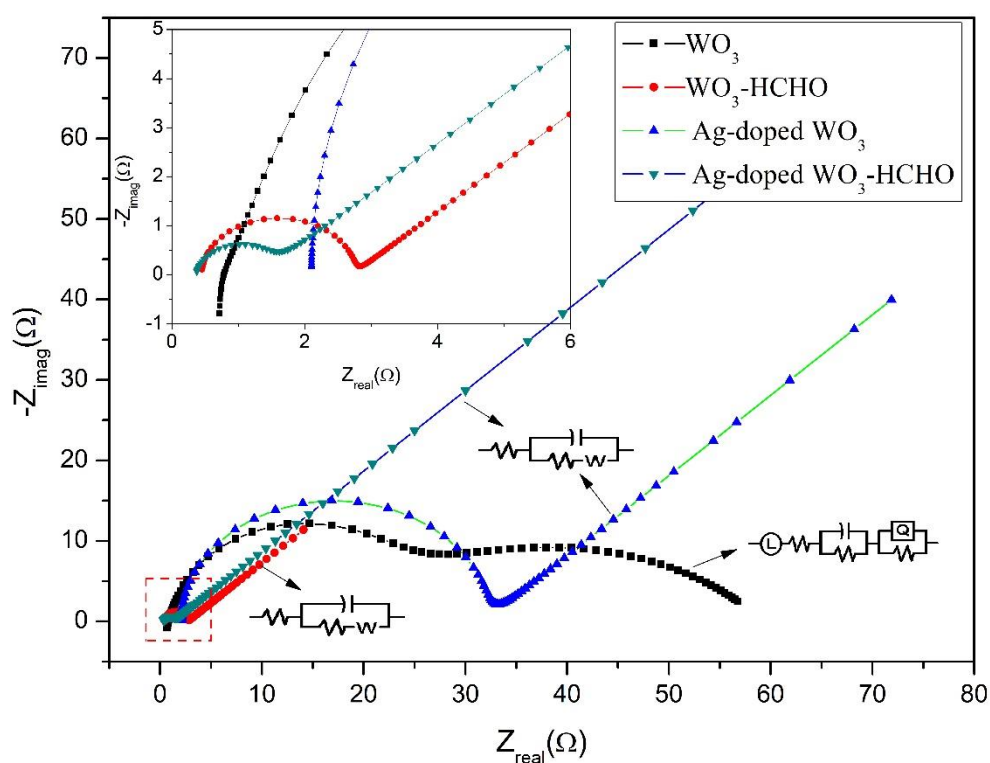

Figure 5. EIS Nyquist spectra of the samples before and after exposure to formaldehyde, the spots correspond to the experimental data, the solid lines stand for the calculated data from the equivalent circuits

Meanwhile, the results manifested that the Ag-doped WO_3 electrode reveals a larger semicircle with a total resistance of ~ 30 Ω in comparison with the pure WO_3 film of ~ 19 Ω, the total resistance was calculated by fitting with equivalent circuit analysis of the impedance data, the corresponding equivalent circuit is depicted in Fig. 5, demonstrating a higher charge carrier resistance [15-16]. This may be due to the formation of hetero-junction after introducing Ag. Furthermore, Fig. 5 also shows that the total resistance of Ag-WO_3 material was reduced to ~ 0.98 Ω after contacting formaldehyde, and the pure WO_3 electrode exhibited a lowered resistance of ~ 2.2 Ω. It can be obtained that the vibration in resistance of Ag-doped WO_3 was approximately 3.5 times higher than the pure WO_3. Thus, enhanced response signal of the gas sensor will be exhibited for gas sensing. Hence, the EIS analysis demonstrates a better sensing response of Ag-doped WO_3 for HCHO detection.

3.3 Gas sensing performances

In addition to the above electrochemical test, gas sensitivity test was also carried out to study the performance changes before and after doping Ag. It's clearly to see from Fig .6 that the sensing response of WO_3 was enhanced after adding noble metal Ag to HCHO, the operating temperature of the gas sensor was significantly reduced at the same time. The response of Ag-WO_3 was as high as 10.3 at 250 °C, which was higher than the pure WO_3 of 6.5 at working temperature of 350 °C. More obviously, Fig. 7 displays that the response/recovery rate of the WO_3 has increased significantly owing to the assistance of Ag. The response time of Ag-doped WO_3 sensor to 100 ppm HCHO was calculated to 3 s, which was shorter than the pure one (9 s), meanwhile, the recovery time of the Ag-doped WO_3 reduced from 6 s to 3 s. The improved sensing performances may be attributed to the hetero-structure and the catalysis role of Ag nanoparticles. The corresponding detailed explanation is given in the following section.
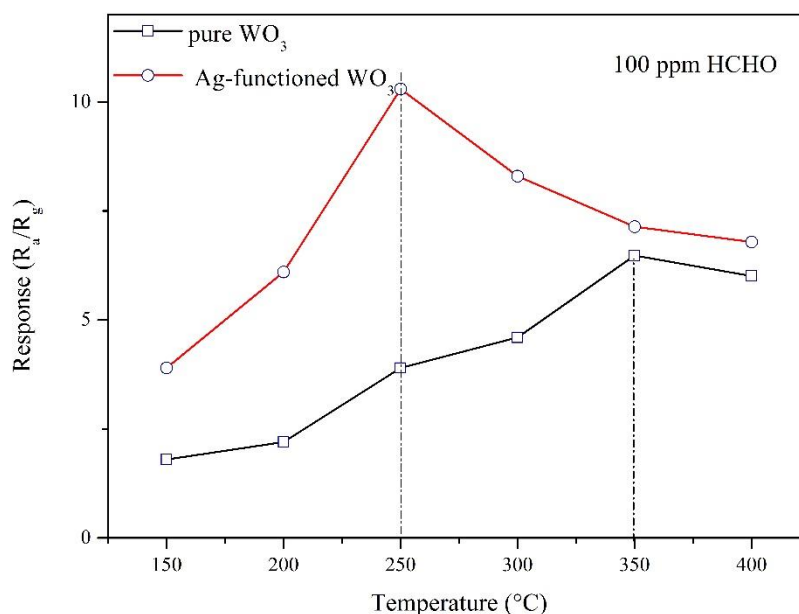
Figure 6. Gas response of pure WO_3 and Ag-doped WO_3 samples at different operating temperature to 100 ppm formaldehyde
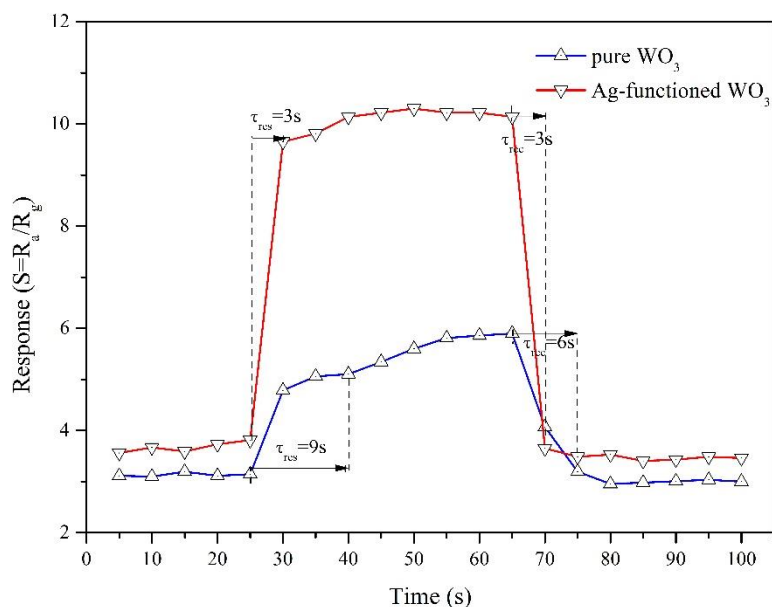
Figure 7. Response/Recovery time of pure WO_3 and Ag-doped WO_3 samples at 250 °C to 100 ppm formaldehyde

A comparison of HCHO gas sensing performances in this work with some reported literatures was shown in Table 1. Obviously, Ag-doped 3D WO_3 based sensors were considered to have advantages on response/recovery rate, gas sensitivity and operating temperature for monitoring formaldehyde. It is important that the facile preparation method makes the material easier to produce in industry and and it will become a promising formaldehyde gas sensitive material in practical application.

Table 1. A comparison of HCHO sensing performances in this work with previous literatures.

Sensing material	Synthesis method	Sensitivity	Operating temperature (°C)	Response/ Recovery time (s)	Reference
Au modified WO_3 nanorods	Ion exchange method	2.0 (50 ppm)	290	/	[17]
6.67 % Ce-Sn_3O_4	Hydrothermal	5.5 (100 ppm)	200	4/8	[18]
NiO nanowires	Hydrothermal	~13 (100 ppm)	200	24/20	[19]
In_2O_3 nanoribbons	Electro-spinning	3.13 (100 ppm)	340	18/17	[20]
ZnO nanoplates	Hydrothermal	1.88 (100 ppm)	RT (UV-light)	97/86	[21]
ZnO nanoflowers	Hydrothermal	4.95 (100 ppm)	RT (UV-light)	44/104	[21]
Ag-doped 3D WO_3	Hydrothermal	10.3 (100ppm)	250	3/3	This work

RT= room temperature.

3.4 Gas sensing mechanism

Based on above results, it's obvious to obtain that the introduction of precious metal silver improves the gas sensing properties of the material to formaldehyde. The improvement of gas sensing characteristics after doping Ag can be explained by the space charge region theory and the catalysis of silver.

Firstly, based on metal-semiconductor (M-S) heterojunction theory, Ag NPs-WO_3 M-S junctions are generated to reach a uniform Femi-level owing to the difference in work functions. As a result, the free electrons migrate from the conduction band of WO_3 to Ag concurrently, causing a depletion layer region around the interface. The active heterogeneous regions promote the physico-chemical adsorption process of oxygen molecules and convert into oxygen ions even at low temperature, which significantly enhances electron transport, thereby improving the sensing response to target gas [22-25].

Secondly, as a noble metal with strong catalytic action, silver can promote the reducing formaldehyde molecules convert into the target product even at a lower operating temperature. The oxygen molecules adjacent to the hetero-junction are more inclined to dissociate into negative oxygen ions on the surface of the Ag which possess a stronger oxidizing capacity. Furthermore, on account of the presence of Ag, the bond dissociation energy of the reactions occurred on surface might be reduced, hence HCHO molecules could be more likely dissociated into target products, meanwhile, the response/recovery speed also increased compared with un-doped WO_3. As a consequence, the Ag-doped WO_3 can be a promising material in HCHO gas-sensing practical application [23-28].

4. CONCLUSIONS

In summary, a simple hydrothermal route combined with a wet dipping process was successfully carried out to synthesis Ag-doped 3D WO_3 HCHO sensing material. The electrochemical behavior and gas sensing results of the pure WO_3 and Ag-doped WO_3 demonstrated that the vibration in resistance of Ag-doped WO_3 was approximately 3.5 times higher than the pure one after contacting formalin, and a higher response of 10.3 to 100 ppm HCHO was obtained at working temperature of 250 °C, which was better than the pure WO_3 of 6.5 at 350 °C, the response/ recovery time was shorted to 3 s/3 s after doping Ag .The enhancement of gas sensing characteristics of WO_3 by doping Ag could be attributed to the hetero-structure and the catalysis role of silver. The Ag-doped WO_3 can be promising in HCHO gas-sensing practical application.

References

1. Y. He, H.H. Li, X.X. Zou, N. Bai, Y.Y. Gao, M.H. Fan and G.D. Li, *Sens. Actuator B-Chem.*, 244 (2017) 475.
2. Y.L. Liu, J. Huang, J.D. Yang and S.R. Wang, *Solid-State Electron.*, 130 (2017) 20.
3. H. Yu, T.Y. Yang, Z.Y. Wang, Z.F. Li, B.X. Xiao, Q. Zhao and M.Z. Zhang, *J. Alloy. Compd.*, 724 (2017) 121.
4. Y.X. Li, N. Chen, D.Y. Deng, X.X. Xing, X.C. Xiao and Y.D. Wang, *Sens. Actuator B-Chem.*, 238 (2017) 264.
5. S.L. Bai, J. Guo, X. Xiang, R.X. Luo, D.Q. Li, A.F. Chen and C.C. Liu, *Sens. Actuator B-Chem.*, 245 (2017) 359.
6. N. Han, X.F. Wu, D.W. Zhang, G.L. Shen, H.D. Liu and Y.F. Chen, *Sens. Actuator B-Chem.*, 152 (2011) 324.
7. A.B. Yadav and S. Jit, *Int. J. Hydrog. Energy*, 42 (2017) 786.
8. C.H. Feng, C. Wang, P.F. Cheng, X. Li, B. Wang, Y.H. Guan, J. Ma, H. Zhang, Y.F. Sun, P. Sun, J. Zheng and G.Y. Lu, *Sens. Actuator B-Chem.*, 221 (2015) 434.
9. S. Kundu, I. Subramanian, M. Narjinary and R. Manna, *Ceram. Int.*, 42 (2016) 7309.
10. S.X. Cao and H. Chen, *J. Alloy. Compd.*, 702 (2017) 644.
11. H.Y. Du, J. Wang, M.Y. Su, P.J. Yao, Y.G. Zheng and N.S. Yu, *Sens. Actuator B-Chem.*, 166–167 (2012) 746.
12. W. Zeng, H. Zhang and Z. C. Wang, *Appl. Surf. Sci.*, 347 (2015) 73.
13. P.Q. Wu, Z.F. Liu, D. Chen, M. Zhou and J.D. Wei, *Appl. Surf. Sci.*, 440 (2018) 1101.
14. Z.C. Yin and Y.Y. Bu, *Chem. Eng. J.*, 345 (2018) 165.
15. C.Y. Wang, X. Zhang, Q. Rong, N.N. Hou and H.Q. Yu, *Chemosphere*, 204 (2018) 202.
16. L. Manjakkal, B. Sakthivel, N. Gopalakrishnan and R. Dahiya, *Sens. Actuator B-Chem.*, 263 (2018) 50.
17. C. Dong, Q. Li, G. Chen, X.C. Xiao, Y.D. Wang, *Sens. Actuator B-Chem.*, 220 (2015) 171.
18. X.H. Ma, J.L. Shen, D.X. Hu, L. Sun, Y. Chen, M. Liu, C.N. Li, S.P. Ruan, *J. Alloy. Compd.*, 726 (2017) 1092.
19. Z. W. Li, *Vacuum,* 143 (2017) 50.
20. J.B. Cui, L.Q. Shi, T.F. Xie, D.J. Wang, Y.H. Lin, *Sens. Actuator B-Chem.*, 227 (2016) 220.
21. C.-S. Lee, J.-H. Choi, Y.-H. Park, *J. Ind. Eng. Chem.*, 29 (2015) 321.
22. T. Liu, J.Y. Liu, Q. Liu, R.M. Liu, H.Q. Zhang, X.Y. Jing, *Sens. Actuator B-Chem.*, 250 (2017) 111-120.
23. H. Yu, J. Li, Y. Tian, Z. Li, *J. Alloy. Compd.*, 765 (2018) 624.
24. C.H. Feng, C. Wang, P.F. Cheng, X. Li, B. Wang, Y.H. Guan, J. Ma, H. Zhang, Y.F. Sun, P. Sun, J. Zheng, G.Y. Lu, *Sens. Actuator B-Chem.*, 221 (2015) 434.
25. J. Cao, Z.Y. Wang, R. Wang, S. Liu, T. Fei, L.J. Wang, T. Zhang, *J. Mater. Chem. A*, 3 (2015) 5635.
26. Z.P. Li, Y.J. Fan, J.H. Zhan, *Eur. J. Inorg. Chem.,* 21 (2010) 3348.
27. Y.Y. Cao, Y. He, X.X. Zou, G.D. Li, *Sens. Actuator B-Chem.*, 252 (2017) 232.
28. S.M. Li, L.X. Zhang, M.Y. Zhu, G.J. Ji, L.X. Zhao, J. Yin, L.J. Bie, *Sens. Actuator B-Chem.*, 249 (2017) 611.